Journal of Applied Polymer Science

# Photodegradation of Some Low-Density Polyethylene–Montmorillonite Nanocomposites Containing an Oligomeric Compatibilizer

**Wael A. Al Abdulla,[1] David J. T. Hill,[2] Andrew K. Whittaker[1,3]**

[1]Australian Institute for Bioengineering and Nanotechnology, University of Queensland, Brisbane, Queensland 4072, Australia
[2]School of Chemistry and Molecular Biosciences, University of Queensland, Brisbane, Queensland 4072, Australia
[3]Centre for Magnetic Resonance, University of Queensland, Brisbane, Queensland 4072, Australia
Correspondence to: W. A. Al Abdulla (E-mail: w.ghafor@uq.edu.au)

**ABSTRACT:** The photo-oxidation behavior at the exposed surfaces of maleated low-density polyethylene [LDPE poly(ethylene-*co*-butylacrylate-*co*-maleic anhydride) (PEBAMA)] and montmorillonite (MMT) composites was studied using attenuated total reflection Fourier transform infrared spectroscopy, X-ray diffraction (XRD), transmission electron microscopy (TEM), and mechanical testing. Two different MMT clays were used with the maleated polyethylene, an unmodified clay, MMT, and an organically modified montmorillonite (OMMT) clay which was significantly exfoliated in the composite. The morphologies of sample films were examined by XRD and TEM. The results were explained in terms of the effect of the compatibilizing agent PEBAMA on the clay dispersion. It was found that the OMMT particles were exfoliated in the polymer matrix in the presence of the PEBAMA, whereas the MMT clay particles were agglomerated in this matrix. Both mechanical and spectroscopic analyses showed that the rates of photo oxidative degradation of the LDPE-PEBAMA–OMMT were higher than those for LDPE and LDPE-PEBAMA–MMT. The acceleration of the photo-oxidative degradation for LDPE-PEBAMA–OMMT is attributed to the effects of the compatibilizer and the organic modifier in the composite. © 2014 Wiley Periodicals, Inc. J. Appl. Polym. Sci. **2014**, *131*, 40788.

**KEYWORDS:** clay; compatibilization; composites; degradation; polyolefins

Received 29 January 2014; accepted 29 March 2014
**DOI: 10.1002/app.40788**

## INTRODUCTION

Over the past few years there has been intense interest in polymer nanocomposites (PNCs), which are polymers (thermoplastics, thermosets, or elastomers) that have been reinforced with small quantities (usually less than 5% by weight) of nanosized particles having high aspect ratios ($l/h > 300$). These nanocomposites can offer improvements over conventional composites in mechanical, thermal and barrier properties and have significantly reduced flammability.[1] Accordingly, PNCs have attracted great interest from a technological and economic point of view, whether in fundamental research or industry.[1–4]

Interest in polyolefin nanocomposites has emerged due to the promise of improved performance in packaging and engineering applications.[4–8] Polyethylene (PE) is categorized as a low surface energy material, like polypropylene, so it interacts only weakly with mineral surfaces, making the synthesis of polyolefin-mineral nanocomposites by melt compounding difficult.[6] Accordingly, chemical modification of PE resins, in particular by the grafting the PE with pendant anhydride groups, or for some polymers by in situ polymerization, have been used to overcome the problems associated with poor interfacial adhesion between the mineral fillers and the polymer matrix.[3,7]

Another approach to addressing this problem has been to introduce an oligomeric compatibilizer into the composite to achieve better exfoliation of the clay, and so ensure formation of a homogeneously dispersed clay nanocomposite.[9] The use of functionalized PE oligomers containing polar groups is an attractive approach, and maleic anhydride (MA) is the most important comonomer used in this context.[10,11] Several previous studies have indicated the beneficial roles of maleated PE and polypropylene in the exfoliation of clays in olefin composites. In such composites, with three components (polymer matrix, compatibilizer, and modified clay), it has been pointed out that the miscibility between the maleated oligomer and the polymer matrix plays a key role in determining the composite properties.[12,13]

Organoclays are natural clay minerals modified by organic cations and they can be considered as fillers added to increase the composite strength and stiffness. The modifier enhances the compatibility of the clay with the polymer and enlarges the clay

interlayer distance.[7] Clays exhibit rich intercalation chemistry, so the layer surfaces of the clay can be readily chemically modified by ionic surfactants and made more compatible with organic polymers for dispersal of the clay platelets. A strong interfacial interaction between the polymer matrix and the modified clay is considered to be a fundamental requirement in the compounding of these composites.[14] The original clay particles often have micrometer dimensions, but when the clay galleries are exfoliated in a polymer composite the clay sheets have a nanometer thickness.

The degree of exfoliation of the clay in a nanocomposite depends on several factors, including the length of the alkyl group of the clay surface modifier, the level of maleation in the compatibilizer and the type of surfactant modifier. Wang et al.[12] found that exfoliation of the clay in nanocomposites based on linear low-density polyethylene (LLDPE) was promoted when the organic modifier on the clay had more than 16 methylene groups and the maleation level was higher than 0.1 wt %. Osman et al.[14,15] conducted studies on high-density PE nanocomposites and suggested that complete coverage of the surface of the clay by the surfactant, leading to high clay gallery *d*-spacings, favored exfoliation. Hotta and Paul[16] also found better dispersion in nanocomposites of LLDPE for surfactants with two alkyl tails rather than surfactants with a single alkyl tail, because a larger *d*-spacing in the clay was caused by the bulkier surfactant.

The photo-oxidation of polyolefins has been extensively studied over the past 50 years as it is a very important consideration in the processing and utilization of these polymers. Studies have principally attributed the degradation to the formation of polymer hydroperoxides during synthesis or processing, and the decomposition of the hydroperoxides on subsequent thermal or ultraviolet (UV) exposure. The studies have focused on the mechanisms of hydroperoxide formation, their fate when the polymers are in use and the roles of catalyst residues and adventitious impurities in hydroperoxide formation and degradation reactions. It has been shown that the rate of photo-oxidation of LDPE is enhanced in the presence of natural clays.[17] Natural clays contain Fe(II)/Fe(III), for example, and these are known to accelerate the degradation of hydroperoxides,[17] so leading to more rapid oxidative chain scission in the presence of clay particles. It is believed that some hydroperoxides and other photoactive species are formed in PEs by undesirable side reactions that occur during synthesis or processing of polyolefins, and that these act as the initiators for PE photo-oxidation. The results of an enormous body of work and the methods adopted to minimize the effects of these photoactive species on the useful life times of PEs have been periodically reviewed.[3,4,18–23]

The rate of photo-oxidation of clay composites depends on several factors, including the extent of intercalation or exfoliation of the clay layers, the presence of transition-metal ions and the presence of active sites on the clay surfaces, amongst other considerations.[24] Carbonyl groups are known to be photoactive and their presence in a composite can lead to the degradation of PEs with the formation of new functional groups and to chain scission reactions.[25]

Clough and coworkers[26] reported that at least 11 oxidation products are formed during polyolefin photo-oxidation, and that these products fall into the general categories of ketones, carboxylic acids, esters, peresters, ketals, hemiketals, peroxides, and alcohols. Salvalaggio et al.[27] used Fourier transform infrared (FTIR) transmission spectroscopy to study oxidation of LDPE in an oxygen atmosphere and they used spectral curve fitting to identify 10 components that absorb in the FTIR carbonyl region of 1650–1800 $cm^{-1}$. They assigned these components to a variety of ketones and aldehydes, carboxylic acids and esters, peracids and peresters, lactones, and unsaturated groups. Thus, the methods of initiation of oxidation of PEs in air and the photo-oxidation products of polyolefin degradation have been well characterized, and reaction sequences have been formulated to account for byproduct formation.[18,19,28,29]

Recently,[30] we found that the extent of oxidative degradation of LDPE was slightly greater when montmorillonite (MMT) was present in a composite and was greatest for a blend of LDPE and organically modified montmorillonite (OMMT). The distribution of the photo-oxidation products was somewhat modified in the presence of MMT and OMMT in comparison with virgin LDPE, with the yield of acidic products higher and the yield of double bonds lower than for LDPE. However, the MMT and OMMT were not exfoliated in these composites.

This article is an extension to this earlier work,[19] wherein the photo-oxidation behavior of maleated LDPE–clay composites is investigated. A poly(ethylene-*co*-butylacrylate-*co*-maleic anhydride) (PEBAMA) compatibilizer was blended with the LDPE. Two different nanoclays, MMT and OMMT, were used to produce PE–clay composites, and their influence on the photo-oxidative degradation and mechanical properties of the composites formed with the maleated LDPE was evaluated.

## EXPERIMENTAL

Alkathene LDN248, LDPE, was obtained from Qenos, Australia. Alkathene is an extrusion grade product with a melt flow index of 8.5 at 190°C for a mass of 2.16 kg and it has a density of 0.922 g $cm^{-3}$. No additional antioxidant or other additives were added to the LDPE. The MMT clay samples were obtained from Southern Clay Products. The PEBAMA compatibilizer with a melt index of 5 g/10 min (190°C/2.16 kg), mp 107°C, density 0.94 g $mL^{-1}$ at 25°C containing 5.5 wt % butylacrylate and 3.5 wt % MA was provided by Sigma-Aldrich Co. The two types of clay utilized in this study, and their properties, were

i. Cloisite®$Na^+$, designated MMT, which is an unmodified natural clay with 90% of the clay particles less than 13 $\mu$m in diameter and with a reported spacing between the clay galleries of $d_{001} = 1.17$ nm.
ii. Cloisite®20A, designated OMMT, which is a modified natural clay with 90% of the clay particles less than 13 $\mu$m in diameter and with a spacing between the clay galleries of $d_{001} = 2.42$ nm.
iii. The surface modifier used in the OMMT is a dimethyl dialkylammonium chloride (see below), with the two long-chain alkyl groups, T, being hydrogenated tallow consisting

of 65% C18, 30% C16, and 5% C14 alkyl chains. The concentration of the modifier in OMMT is 95 meq/100 g.

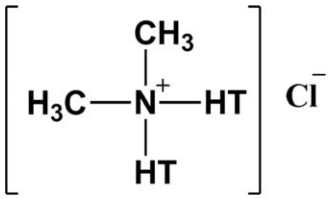

Composite samples were produced by melt compounding LDPE with MMT or OMMT (1, 3, and 5 wt %) and PEBAMA. The weight ratio of PEBAMA to clay was maintained at 4 : 1 in all of the samples. The MMT composites are designated LDPE-PEBAMA–MMT-1%, LDPE-PEBAMA–MMT-3%, and LDPE-PEBAMA–MMT-5%, respectively, and with OMMT are designated LDPE-PEBAMA–OMMT-1%, LDPE-PEBAMA–OMMT-3%, and LDPE-PEBAMA–OMMT-5%, respectively. Samples of virgin LDPE and LDPE with 20% PEBAMA (designated LDPE-PEBAMA) were also prepared for comparison purposes.

The clays and PEBAMA were blended with the LDPE in a Brabender blender model PL 2000 at a temperature of 170°C using a mixing frequency of 60 $min^{-1}$ and a mixing time of 5 min. These blending conditions were chosen so as to minimize any decomposition of the polymer or the organic modifier in the OMMT. After blending, virgin LDPE and the composite mixtures were pressed into sheets of 1 mm thickness. This was done in a hydraulic press fitted with stainless steel compression plates and using a load of 30 ton at 210°C. Then, the polymer sheets were cooled in the compression mold to ambient temperature by circulating water through the heater plates. Samples of an appropriate size for UV exposure and mechanical analysis were cut from these sheets.

X-ray diffraction (XRD) and transmission electron microscopy (TEM) were used to observe the dispersion and degree of aggregation of the clay particles and the extent of exfoliation of the clay layers in the composites. The XRD analyses were performed with a Bruker D8 Advance instrument that was equipped with a graphite monochromator, a copper target and a scintillation counter detector. The analyses were performed on powdered clay samples over a $2\theta$ range of 2–10° at intervals of 0.02° with a step time of 20.3 s. The XRD data were later processed by smoothing to reduce noise.

TEM measurements were carried out using a Phillips CM20 instrument and an acceleration voltage of 120 kV. For this analysis ultrathin sections of the composites of 70 nm thicknesses were cut from the compression molded samples using an ultramicrotome Leica EM FCS attached to a closed chamber with circulating liquid $N_2$, which is designed for use in preparing thin layers for FTIR attenuated total reflection (ATR) measurements.

For the degradation studies, the samples were exposed in air at room temperature to UV light in a Q-Panel Weatherometer fitted with an array of Q-Panel UV–B 313 nm fluorescent tube lamps (no water spraying). The photon flux from the lamp array was measured at the position of the samples during exposure and was 0.15 W $m^{-2}$.

After exposure the chemical changes due to photo-oxidation were monitored by FTIR spectroscopy. The surface spectra were delineated using a Nicolet 5700 FTIR spectrometer fitted with a diamond ATR accessory. The spectra were acquired over the wavelength range 500–4500 $cm^{-1}$ and corrected for the background. The spectra were collected at room temperature at a resolution of 4 $cm^{-1}$ and averaged over a total of 64 scans to improve the signal-to-noise ratio. All of the spectra were indexed using the intensity of the C–H peak at 1461 $cm^{-1}$.

The mechanical properties of the nanocomposites were measured at room temperature according to ASTM D638 using an Instron Model 5584 universal testing machine. Samples were cut from the sheet using a dumbbell cutter die to ASTM D638 standards with a gauge width of 2.5 mm and gauge length of 15 mm. Tension mode with a cross head speed of 5 cm $min^{-1}$ and a 100-N load cell were used in the measurements. The average of three to five replicates for each sample was calculated and the replicates used to estimate the precision of the reported data.

## RESULTS AND DISCUSSION

### Characterization of PE–Clay Nanocomposites

The XRD profile of the OMMT clay is shown in Figure 1(A). The $d_{001}$ spacing (peak $2\theta = 3.3°$) between the OMMT clay galleries was calculated to be $2.5 \pm 0.1$ nm. This spacing is slightly greater than that reported by the manufacturer (2.42 nm), but is within experimental error of this value. The XRD also has a small peak at $2\theta = 7.2°$, indicating that a small proportion of the clay layers (about 12%) have a spacing of about 1.2 nm, indicating that the tetra alkylammonium chloride modifier has not penetrated the layers of these clay particles. The XRD of LDPE-PEBAMA–OMMT-5% is shown in Figure 1(A) and has no significant 001 diffraction peak. This is an indication that the clay layers in this composite are significantly exfoliated in the polymer matrix and dispersed as nanosized clay sheets. The origin of the small peak at $2\theta = 5.2$ is uncertain, but it could, for example, arise from a reflection of a peak observed at a lower angle. The presence of the unmodified clay particles can also be seen at $2\theta \approx 7.5$.

An XRD diffractogram of the MMT clay particles is shown in Figure 1(B) and yielded a separation of the clay galleries of $1.11 \pm 0.03$ nm, in close agreement with that reported by the manufacturer, 1.17 nm. The XRD diffractogram of the LDPE-PEBAMA–MMT-5% blend also yielded a gallery spacing of $1.11 \pm 0.02$ nm, even though PEBAMA was present. Thus the MMT is dispersed as micron-sized particles in the LDPE matrix, with negligible intercalation of polymer chains into the clay.

TEM measurements were used to confirm the dispersion of clay particles in the PNCs. Figure 2 shows the TEM images of LDPE-PEBAMA–MMT-5% and LDPE-PEBAMA–OMMT-5%. Figure 2(A) shows that irregular sized MMT particles are present in the MMT composite, indicating poor clay dispersion, particle aggregation, and no exfoliation of the clay sheets. However, the images in Figure 2(B) for the OMMT blend clearly show that the stacked layer structures of the clay have been

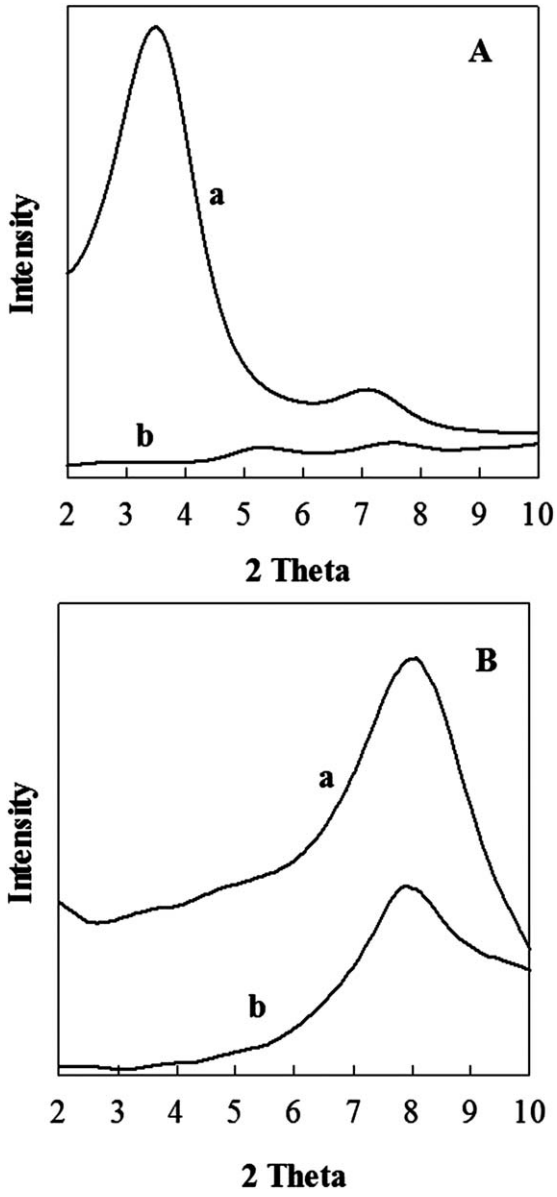


**Figure 1.** X-ray diffractograms in the range of $2\theta$ from 2° to 10°. (A; a) virgin OMMT and (b) OMMT in an LDPE-PEBAMA–OMMT-5% composite and (B; a) virgin MMT and (b) MMT in an LDPE-PEBAMA–MMT-5% composite.

separated into thin exfoliated sheets of OMMT. The exfoliated clay sheets are well dispersed in the matrix polymer.

In a previous study,[31] OMMT clay was found to be dispersed as micron sized particles in a LDPE matrix when no compatibilizer was present, with minimal intercalation of the olefin chains between the clay galleries. In that study, there was no significant exfoliation of the OMMT clay layers into the polymer matrix. However, in this present work the interaction between the polar groups of the PEBAMA compatibilizer and the charged surfactant molecules on the clay surface leads to greater exfoliation of the clay layers.[32]

In summary, the composites that do not contain the organically modified clay and compatibilizer exhibit no evidence of exfoliation in their TEM micrographs, while those with the organic modifier and compatibilizer are extensively exfoliated. These observations are consistent with the conclusions drawn from the XRD study.

### FTIR Studies of UV Degradation

Typical ATR-FTIR spectra of virgin LDPE, LDPE-PEBAMA and the clay composites before UV exposure are shown in Figure 3. The peaks in the spectra at 1471 and 1461 $cm^{-1}$ and at 731 and 721 $cm^{-1}$ arise from the methylene groups of the LDPE and PEBAMA. The peaks in the spectrum of LDPE-PEBAMA at 1780 and 1739 $cm^{-1}$ are attributed to the presence of the carbonyl groups of the MA (succinic anhydride segments in the copolymer chain) and butyl acrylate, respectively. The peak in the spectrum at 1780 $cm^{-1}$ corresponds to the anti-symmetric carbonyl stretching vibration of the cyclic anhydride group. The symmetric carbonyl stretching vibration of the anhydride appears at 1855 $cm^{-1}$, but is of very low intensity. A further characteristic band for the cyclic anhydride is the C–O–C band that appears at 1220 $cm^{-1}$. The peaks in the spectra between 1000 $cm^{-1}$ and 1160 $cm^{-1}$ for the composites belong to the modified and nonmodified Cloisite, with the peaks at 1040 and 1050 $cm^{-1}$ corresponding to Si–O–Si stretching vibrations of the clay.[33,34]

New bands appear in the ATR-FTIR spectra of LDPE, LDPE-PEBAMA, LDPE-PEBAMA–MMT-5%, and LDPE-PEBAMA–OMMT-5% after exposure in the Weatherometer. The spectra in Figure 4 show the appearance of new peaks in the carbonyl region for LDPE at different exposure times. The broad nature of these carbonyl bands and their profiles, which show the presence of multiple peaks, indicate that a number of different carbonyl species are present in the photo-oxidized films, most likely including ketones, carboxylic acids, esters, peresters, ketals, and hemiketals as reported by others.[35–37] The intensity of the carbonyl band builds up with photolysis time, as demonstrated in Figure 4, but there is little change in the overall band profile as degradation proceeds.

It is well accepted that the photo-oxidation process in LDPE occurs due to the presence of adventitious photolabile alkyl hydroperoxides formed during synthesis and processing that then decay on photolysis via a branching chain mechanism. The hydroperoxide decay reaction occurs with the formation of radical sites on the polymer chains, followed by the addition of oxygen at these sites leading to formation of new hydroperoxide functionalities.[35–37] Thus the oxidation process is autocatalytic.

The profiles of the new carbonyl peaks that appear in the spectra of LDPE-PEBAMA, LDPE-PEBAMA–MMT-5%, and LDPE-PEBAMA–OMMT-5% on UV exposure are similar to those found for LDPE (see Figure 5). However, the band intensities for the composites at any photolysis time depend on the clay concentration, as well as on the extent of exfoliation of the clay galleries. The carbonyl band intensities were found to increase with increasing clay content for both the MMT and OMMT composites at a particular exposure time, as demonstrated in Figure 5 for an exposure time of 165 h. The intensity of the band for the LDPE-PEBAMA–MMT composites increases linearly with the MMT content, but for the LDPE-PEBAMA–

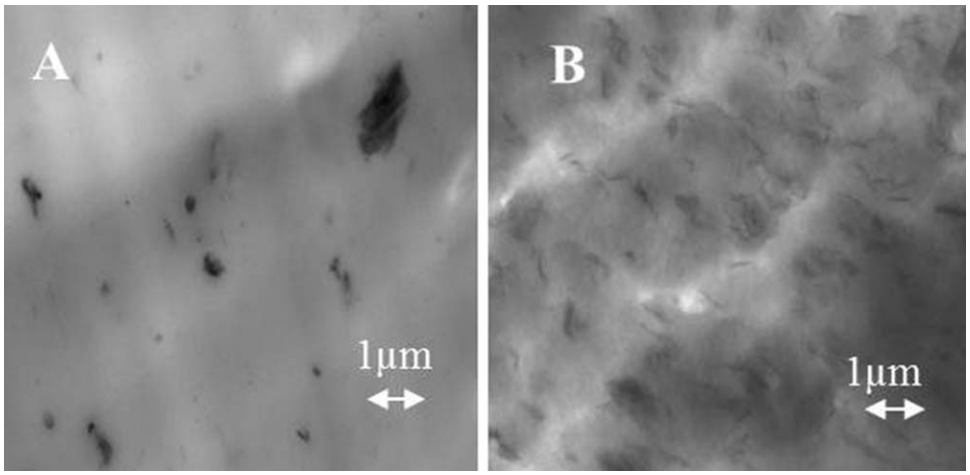


**Figure 2.** TEM micrographs of ultra-thin sections of (A) LDPE-PEBAMA–MMT-5% and (B) LDPE-PEBAMA–OMMT-5%. Scale bar is 1 $\mu$m.

OMMT the rate of increase was greater at lower OMMT concentrations, presumably as a result of the exfoliation of the clay particles, as elaborated upon below. Figure 5 also shows that the extent of carbonyl formation in the presence 1% OMMT is about three times larger than that in the presence of 1% MMT, based on the area under the carbonyl peak or the peak height. However at higher clay concentrations, the difference becomes smaller and is only ≈1.5 times more for clay concentrations of 5%. Similar observations have been made by Sanchez-Valdes for LDPE blended with a MA-grafted LDPE compatibilizer and OMMT (20A).[38]

Figure 6 shows typical difference spectra obtained by subtraction of the spectrum of the samples recorded before exposure from those recorded after 333 hrs exposure. The spectra have been indexed using the methylene peak for LDPE at 1461 $cm^{-1}$. This ensures that the ATR spectra are representative of the same amount of LDPE in each case. The C–O bands in the difference spectra (1150–1250 $cm^{-1}$) are not very useful for identifying the photo-oxidation products, so have not been shown in Figure 6, but the carbonyl bands (1660–1800 $cm^{-1}$) have been widely used for this purpose. The presence of vinyl groups after photolysis can also be clearly identified by the new band at 909 $cm^{-1}$. The new carbonyl and vinyl bands in the spectra of the samples each have similar profiles, but the intensities vary from sample to sample.

In Figure 7(A,B), the intensities of the carbonyl and vinyl peaks are plotted versus the photolysis time for LDPE, LDPE-PEBAMA, LDPE-PEBAMA–MMT-5%, and LDPE-PEBAMA–OMMT-5%. The LDPE-PEBAMA, LDPE-PEBAMA–MMT-5% and LDPE-PEBAMA–OMMT-5% contain the same concentration of PEBAMA, namely 20 wt %. Over a period of 333 h, the carbonyl peak intensities shown in Figure 7(A) are seen to increase approximately linearly with time (correlation coefficients $> 0.95$), as do the intensities of the vinyl peak intensities in Figure 7(B). The slopes of these plots have been calculated relative to those for LDPE and the results are summarized in Table I.

From Table I, the relative rate of oxidation assessed by carbonyl group formation in LDPE-PEBAMA is seen to be 1.4 times that

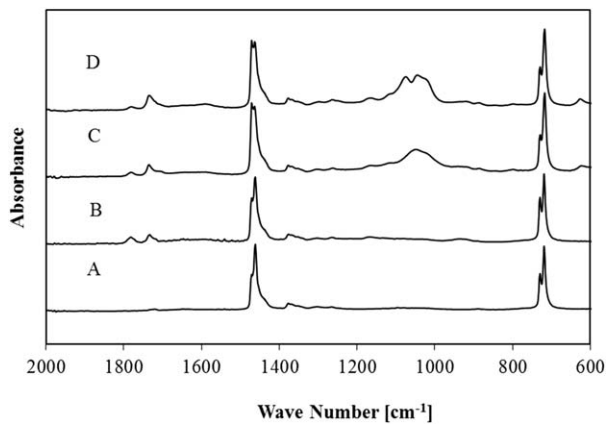


**Figure 3.** ATR-FTIR spectra for (A) LDPE, (B) LDPE-PEBAMA, (C) LDPE-PEBAMA–MMT-5%, and (D) LDPE-PEBAMA–OMMT-5% before UV irradiation. Spectra are offset for clarity.

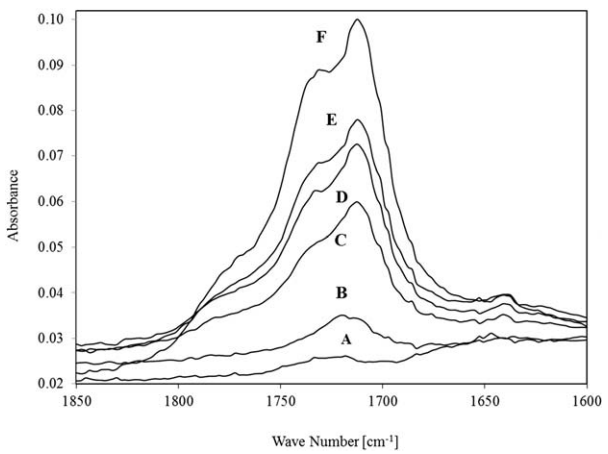


**Figure 4.** ATR-FTIR spectra of carbonyl band of LDPE during photo-oxidation. (A) 0.0 h, (B) 71 h, (C) 168 h, (D) 193 h, (E) 265 h, and (F) 367 h. The spectra are indexed on the methylene peak at 1471 $cm^{-1}$.

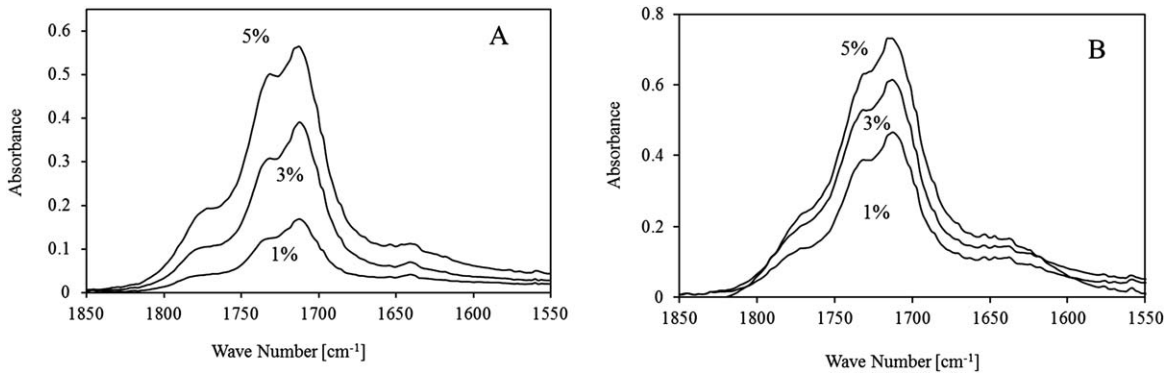


**Figure 5.** FTIR-ATR spectra of the carbonyl bands for the composite samples with increasing clay concentrations (A) LDPE-PEBAMA–OMMT and (B) LDPE-PEBAMA–MMT exposed to UV radiation for 165 h. The spectra have been indexed to the methylene peak at 1471 $cm^{-1}$.

for LDPE, which can be attributed to the presence of the carbonyl groups in the compatibilizer.[25] In the presence of 5% MMT, the relative rate of 1.4 times is the same as that for LDPE-PEBAMA, but when 5% OMMT is present the relative rate is 1.8 times that for LDPE. The significant increase for LDPE-PEBAMA–OMMT-5% is attributed to the exfoliation of the clay particles and the presence of the clay modifier, as discussed below.

The rate of formation of vinyl groups in LDPE-PEBMA is also much greater than that observed for LDPE, and the rate enhancement of 1.3 times is similar to that observed for the relative rate of formation of carbonyl groups (1.4 times). Addition of MMT results in a slight decrease in the relative rate of double bond formation to a value of 1.2 for LDPE-PEBAMA–MMT-5%, but on the other hand, addition of OMMT enhances the rate to 1.7 times that for LDPE in the case of LDPE-PEBAMA–OMMT-5%.

Vinyl group formation is a characteristic of the photo-oxidation of PE, but not of thermal oxidation. Photoexcitation of in-chain ketones is believed to be responsible for the formation of these unsaturated groups through a Norrish Type II mechanism. Degradation via a Norrish Type I mechanism leads to the formation

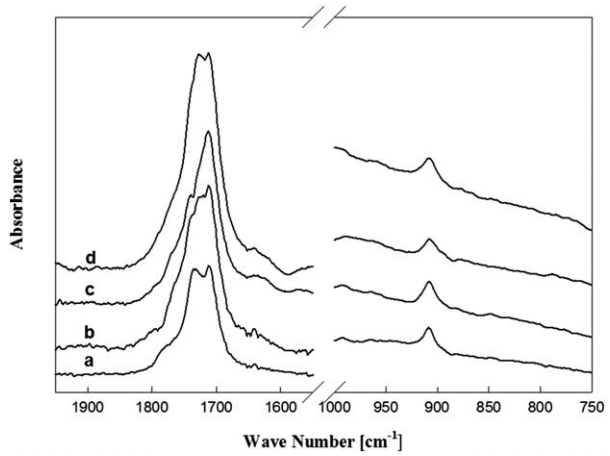


**Figure 6.** ATR-FTIR difference spectra for (a) LDPE, (b) LDPE-PEBAMA, (c) LDPE-PEBAMA–MMT-5%, and (d) LDPE-PEBAMA–OMMT-5%. The difference spectra are for 333 h minus 0 h and are offset for clarity.

of chain end carbonyl and alkyl radicals. Guillet[39] have reported that the photolytic quantum yields for the Norrish Type I and Type II processes in the photo degradation of PE are approximately the same. Thus the presence of the PEBAMA compatibilizer in the LDPE significantly increases the photo degradation rate and in the presence of OMMT, with the clay galleries exfoliated, the degradation rate is further increased substantially.

Increases in the photodegradation rates for polyolefin–clay mineral composites have been observed by other workers[24,40–46] who have attributed the higher rates variously to the deposition of any anti-oxidant present in the polyolefin onto the polar mineral surface, to catalytic effects of iron impurities in the clay minerals or to the generation of radicals by oxidation of the alkyl chain of the clay modifier. It has also been proposed that the photo-oxidation of the modifier can lead to the formation of catalytic sites on the surface of the silicate layers of the clay.[24] It is likely that the clay surfaces also act as scavengers for any negatively charged polar species that are produced during the photo-oxidation process.

Thus, the main reasons for the increased photodegradation rates for the OMMT composites over that for LDPE are firstly the presence of the PEBAMA compatibilizer and secondly the exfoliation of the clay galleries with their surfaces coated by the modifier. The degradation of both the compatibilizer and the modifier, as well as the formation of acidic sites on the clay, probably all play a role.[24,47] The precursors for the degradation of the LDPE are formed during the synthesis and blending processes, and the degradation process is initiated on exposure of the composites to UV light. For these reasons the clay content and the choice and amount of compatibilizer used are important considerations when assessing the lifetimes of LDPE–clay composites in a UV environment. The mixing conditions should also be carefully chosen to minimize or preferably to avoid any decomposition of the components during blending.

Although the principal focus of this study was the photo-oxidation at the exposed surfaces of the polymer matrices, oxidation of the internal bulk polymer was also investigated. To examine the bulk, thin slices of the polymer matrices were cut at right angles to the sample surface, and the interiors of these slices were examined by ATR–FTIR analysis. The new bands that appeared in the ATR spectra of the bulk of the LDPE,

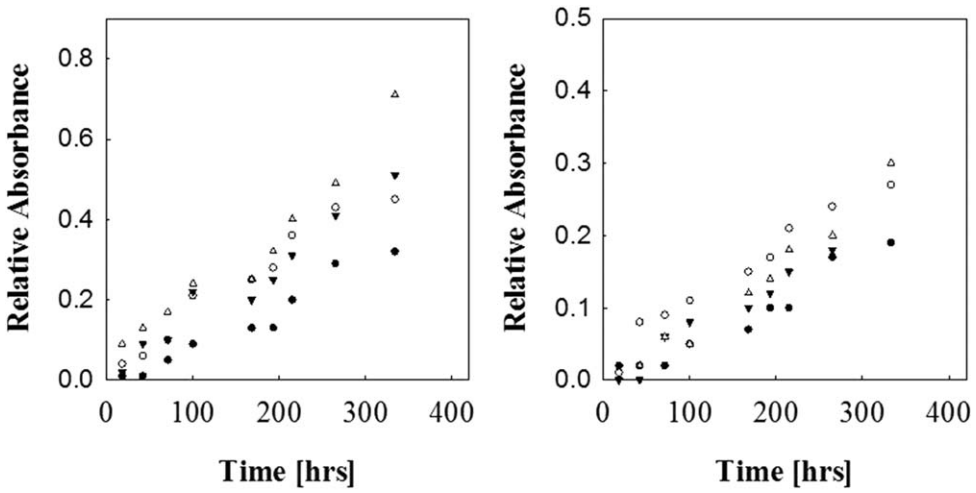


**Figure 7.** The time dependence of the increase in absorbance of (A) the carbonyl band at 1732 $cm^{-1}$ and (B) the vinyl band at 909 $cm^{-1}$ relative to the absorbance of the methylene band at 1471 $cm^{-1}$. LDPE •, LDPE-PEBAMA ○, LDPE-PEBAMA–MMT-5% ▼, and LDPE-PEBAMA–OMMT-5% ▽.

LDPE-PEBAMA–MMT, and LDPE-PEBAMA–OMMT samples following UV photolysis were found to be similar to those in the ATR spectra of the surface of the samples. However, the band intensities were significantly lower for the interiors of the samples, as demonstrated in Figure 8 where the ATR spectra for the carbonyl region of LDPE-PEBAMA–OMMT-5% are presented. Similar observations were made for the UV photolysis of virgin LDPE and LDPE-PEBAMA–MMT-5% composites.

The good correspondence between the band profiles of the two ATR spectra shown in Figure 8 indicates that similar oxidation chemistry occurs at the surface and the interior of the samples, but the rate of oxidation is much higher at the surface. This conclusion is similar to that reported previously[30] for other MMT and OMMT composites of LDPE, and results from the greater availability of oxygen and the higher photon flux at the surface of the samples.

### Mechanical Properties of the Exposed Composites

The manufacturer's specifications for the tensile properties of Alkathene LDN248, LDPE, are Young's modulus = 120–140 MPa, break strain = 250%, and break stress 8–10 MPa.[48] Similar results have been obtained in this work, as demonstrated in Table II. The tensile properties of a typical Alkathene have also been reported elsewhere.[49] Figure 9 shows stress–strain curves for LDPE-PEBAMA–MMT containing 1, 3, and 5% MMT. The strains at failure are in the range 140–190% and are strongly dependent on the clay concentration, decreasing with increasing MMT concentration. The magnitude of the yield stress is about 9 MPa and the break stress 8 MPa. These properties are not significantly affected by the MMT loading.

The LDPE-PEBMA–OMMT composites showed similar shaped stress–strain curves to those for the LDPE-PEBMA–MMT composites, but the properties are different and have been summarized in Table II. The Young's modulus, *E*, of the LDPE-PEBMA–OMMT composites are significantly higher than *E* for LDPE and for the corresponding MMT composites, and *E* increases with increasing OMMT content. This is a well-known behavior of exfoliated clay PE composites, for which the Young's modulus is significantly increased over that for the virgin polymer.[50] The stresses at break, $\sigma$, for the LDPE-PEBMA–OMMT composites are approximately the same as the $\sigma$ for LDPE at all the OMMT loadings. On the other hand the strain at break, $\varepsilon$, decreased systematically with increasing OMMT concentration from a value of 239% at a loading of 0.5 wt % OMMT to 147% for a loading of 5 wt %. The decrease in $\varepsilon$ with increasing

**Table I.** Rate of Increase in the Functional Group Absorbance Relative to that for LDPE During UV Exposure

| Sample | Relative rate of carbonyl formation | Relative rate of vinyl formation |
|---|---|---|
| LDPE-PEBAMA | 1.4 | 1.3 |
| LDPE-PEBMA-MMT-5% | 1.4 | 1.2 |
| LDPE-PEBMA-OMMT-5% | 1.8 | 1.7 |

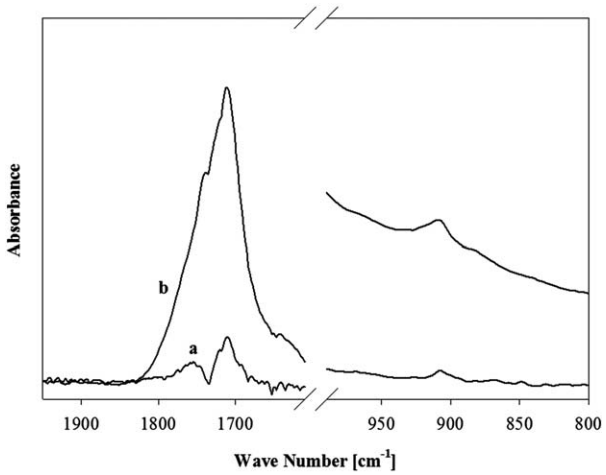


**Figure 8.** FTIR-ATR spectra of LDPE-PEBAMA–OMMT-5% after UV photolysis for 333 h: (a) at the interior (obtained at the center) and (b) at the surface.

**Table II.** Tensile Data for LDPE and LDPE-PEBAMA–OMMT at Time Zero and After 333 h UV Exposure

| Sample | young's modulus (MPa), $t = 0$ | Break stress (MPa), $t = 0$ | Young's modulus (MPa), $t = 333$ | Break stress (MPa), $t = 333$ |
|---|---|---|---|---|
| LDPE | 111 ± 9 | 9.1 ± 0.2 | 103 ± 17 | 4.3 ± 0.5 |
| LDPE-PEBAMA-OMMT-0.5% | 182 ± 25 | 8.8 ± 0.1 | 96.4 ± 15 | 3.9 ± 0.4 |
| LDPE-PEBAMA-OMMT-1% | 229 ± 28 | 9.0 ± 0.2 | 78.6 ± 10 | 4.4 ± 0.2 |
| LDPE-PEBAMA-OMMT-3% | 226 ± 40 | 8.8 ± 0.3 | 125 ± 17 | 4.8 ± 0.3 |
| LDPE-PEBAMA-OMMT-5% | 252 ± 11 | 9.0 ± 0.1 | - | - |

OMMT loading has been observed previously for exfoliated PE clay composites.[51] The mechanical properties of composites are documented to depend on many factors, including the aspect ratio of the filler, the filler loading, the nature of the dispersion of the filler in the matrix and the adhesion at the filler–matrix interface.[32,51]

The tensile properties of the composites were observed to be strongly affected by photo degradation of the LDPE component. Figure 10 shows the stress–strain curves for the LDPE-PEBAMA–MMT composites after 333 h of UV exposure. The dramatic changes in all the tensile properties are clearly obvious from a comparison of the curves in Figures 9 and 10. The tensile properties of the LDPE-PEBAMA–OMMT composites also changed significantly after 333 h of UV exposure and the Young's modulus and break stress are documented in Table II. While the increasing trend in the Young's modulus with increasing clay concentration is similar to that for the unexposed composites, the values are significantly smaller than those of the unexposed samples, and the break stresses are reduced to less than one half of the initial values. The break strains are also reduced significantly to less than 10% of their initial values. At an exposure time of 333 h, the Young's modulus, break stress and break strains of the OMMT composites are comparable to those for LDPE exposed for 333 h, so the property advantages derived from the exfoliated clay have been lost at this exposure time. Indeed, the LDPE-PEBAMA–MMT-5% composite after 333 h of UV exposure was so brittle its tensile properties could not be measured.

## CONCLUSIONS

The clay dispersion and photo-oxidation behaviors of a series of LDPE-PEBAMA–MMT and LDPE-PEBAMA–OMMT blends with different clay concentrations up to 5 wt % have been studied at ambient temperature in air. A low molecular weight copolymer, PEBAMA, was incorporated into the blends as a compatibilizer to enhance exfoliation of the clay galleries in OMMT. No exfoliation occurred for the MMT blends.

The dispersion of the clay in the polymer was studied by XRD and TEM analyses. The LDPE-PEBAMA–MMT composites were shown to contain only micron sized particles of MMT dispersed in the LDPE-PEBAMA matrix, but in the LDPE-PEBAMA–OMMT composites the OMMT clay galleries were significantly exfoliated.

The presence of the PEBAMA compatibilizer and the alkyl ammonium chloride surface modified clay was shown to enhance the rate of UV degradation of the LDPE in the composites. The photo degradation process involves oxidation of the LDPE with the formation of new functional groups, including carbonyl and vinyl groups, as well as polymer chain scission. The carbonyl and vinyl groups that are formed on UV exposure increase in concentration with exposure time, and the rate of increase was shown to be dependent on the presence of the PEBAMA compatibilizer and the organic modifier in the OMMT.

The exfoliation of the OMMT in the blend significantly increased the Young's modulus for the LDPE-PEBAMA–OMMT composites over that for LDPE, and the increase was largest at a 5 wt % clay concentration. The strain at break for the composites decreased with increasing clay content but the break stress was not significantly affected by the presence of the OMMT. On UV exposure the chain scission of LDPE gradually reduces its molecular weight with a consequential loss of the good initial mechanical properties of the blends, and especially for LDPE-PEBAMA–OMMT composite.

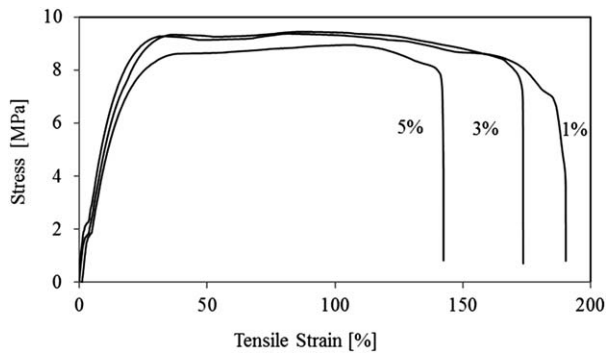


**Figure 9.** Stress–strain curves for LDPE-PEBAMA–MMT with 1, 3, and 5% MMT measured at room temperature.

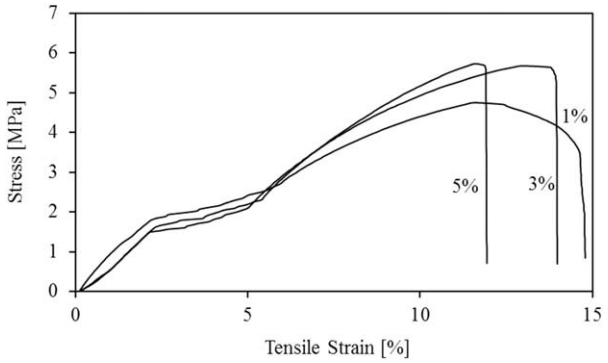


**Figure 10.** Stress–strain curves for LDPE-PEBAMA–MMT with 1, 3, and 5% MMT measured at room temperature after UV irradiation for 333 h.

The precursors of the photo degradation of LDPE are hydroperoxides which are formed during synthesis and processing of the LDPE. Thus it is necessary to minimize the extent of formation of hydroperoxides during processing and blending of the components of these composites.

## ACKNOWLEDGMENTS

The authors would like to thank Professor Darren Martin for providing the clay samples and Dr. Anya J. Yago for performing the XRD measurements. The authors would also like to thank the Australian National Fabrication Facility (ANFF), Queensland Node for access to equipment. Funding from the Australian Research Council (LE0560981, LE0668521, LE0775684, and LE110100028) is gratefully acknowledged.

## REFERENCES

1. Mittal, V. *Materials* **2009**, *2*, 992.
2. Miyagawa, E.; Nitta, K. H.; Tanaka, A. *e-Polymers* **2005**, *5*, 238.
3. Pavlidou, S.; Papaspyrides, C. D. *Prog. Polym. Sci.* **2008**, *33*, 1119.
4. Sinha Ray, S.; Okamoto, M. *Prog. Polym. Sci.* **2003**, *28*, 1539.
5. Gulminea, J. V.; Janissekb, P. R.; Heisec, H. M.; Acelrudd, L. *Polym. Degrad. Stab.* **2003**, *79*, 385.
6. Guoqiang, Q.; Cho, J. W.; Lan, T. Proceedings of Polyolefines; Houston: TX, **2001**.
7. Morawiec, J.; Pawlak, M. S.; Galeski, A.; Piorkowska, E.; Krasnikowa, K. *Eur. Polym. J.* **2005**, *41*, 1115.
8. Kurokawa, Y.; Yasuda, H.; Oya, A. *J. Mater. Sci. Lett.* **1996**, *15*, 1481.
9. LeBaron, P. C.; Pinnavaia, T. J.; Wang, Z. *Appl. Clay Sci.* **1999**, *15*, 11.
10. Shi, D.; Yang, J.; Yao, Z.; Wang, Y.; Huang, H.; Jing, W.; Yin, J.; Costa, G. *Polymer* **2001**, *42*, 5549.
11. Sclavons, M.; Laurent, M.; Devaux, J.; Carlier, V. *Polymer* **2005**, *46*, 8062.
12. Wang, K. H.; Choi, M. H.; Koo, C. M.; Choi, Y. S.; Chung, I. *Polymer* **2001**, *42*, 9819.
13. Reichert, P.; Nitz, H.; Klinke, S.; Brandsch, R.; Thomann, R.; Mülhaupt, R. *Macromol. Mater. Eng.* **2000**, *275*, 8.
14. Osman, M. A.; Rupp, J. E. P.; Suter, U. W. *J. Mater. Chem.* **2005**, *15*, 1298.
15. Osman, M. A.; Rupp, J. E. P.; Suter, U. W. *Polymer* **2005**, *46*, 1653.
16. Hotta, S.; Paul, D. R. *Polymer* **2004**, *45*, 7639.
17. Gournis, D.; Karakassides, M. A.; Petridis, D. *Phys. Chem. Miner.* **2002**, *29*, 155.
18. Carlsson, D. J.; Wiles, D. M. *J. Macromol. Sci. Rev. Macromol. Chem.* **1976**, *14*, 65.
19. Allen, N. S., *Photochemistry* **2007**, *36*, 232.
20. Allen, N. S., *Photochemistry* **2004**, *35*, 206.
21. Allen, N. S., *Photochemistry* **2003**, *34*, 197.
22. Allen, N. S., *Photochemistry* **2002**, *33*, 339.
23. Allen, N. S., *Photochemistry* **2001**, *32*, 343.
24. Qin, H.; Zhao, C.; Zhang, S.; Chen, G.; Yang, M. *Polym. Degrad. Stab.* **2003**, *81*, 497.
25. Laurence Li, S.-K.; Guillet, J. E. *Macromolecules* **1984**, *17*, 41.
26. Mowery, D. M.; Assink, R. A.; Derzon, D. K.; Klamo, S. B.; Bernstein, R.; Clough, R. L. *Radiat. Phys. Chem.* **2007**, *76*, 864.
27. Salvalaggio, M.; Bagatin, R.; Fornaroli, M.; Fanutti, S.; Palmery, S.; Battistel, E. *Polym. Degrad. Stab.* **2006**, *91*, 2775.
28. Adam, T. M.; Celina, M.; Assink, R. A.; Clough, R. L. *Radiat. Phys. Chem.* **2001**, *60*, 121.
29. George, G. A. *Dev. Polym. Degrad.* **1981**, *3*, 173.
30. Ghafor, W. A.; Halley, P. J.; Hill, D. J. T.; Martin, D. J.; Rasoul, F.; Whittaker, A. K. *J. Appl. Polym. Sci.* **2009**, *112*, 381.
31. Zhao, C.; Qin, H.; Gong, F.; Feng, M.; Zhang, S.; Yang, M. *Polym. Degrad. Stab.* **2004**, *87*, 183.
32. Truss, R. W.; Yeow Tay, K. *J. Appl. Polym. Sci.* **2006**, *100*, 3044.
33. Cheng, Q. H.; Lu, Z. X.; Byrne, H. J. *J. Appl. Polym. Sci.* **2009**, *114*, 1820.
34. Liu, H.; Ye, H.; Tang, X. *Appl. Surf. Sci.* **2007**, *254*, 616.
35. Costa, L.; Luda, M. P.; Trossarelli, L. *Polym. Degrad. Stab.* **1997**, *58*, 41.
36. Lacoste, J.; Carlsson, D. *J. Polym. Sci. Part A: Polym. Chem.* **1992**, *30*, 493.
37. Tidjani, A. *Polym. Degrad. Stab.* **2000**, *68*, 465.
38. Sanchez Valdes, S.; Colunga, J. G. M.; Lopez Quintanilla, M. L.; Flores, I. Y.; Garcia Salazar, M. L.; Cantu, C. G. *Polym. Bull.* **2008**, *60*, 829.
39. Guillet, J. *Macromol. Symp.* **1997**, *123*, 209.
40. Mailhot, B.; Morlat, S.; Gardette, J. L.; Boucard, S.; Duchet, J.; Gerard, J. F. *Polym. Degrad. Stab.* **2003**, *82*, 163.
41. Morlat, S.; Mailhot, B.; Gonzalez, D.; Gardette, J. L. *Chem. Mater.* **2004**, *16*, 377.
42. Bocchini, S.; Morlat Therias, S.; Gardette, J. L.; Camino, G. *Polym. Degrad. Stab.* **2007**, *92*, 1847.
43. Leroux, F.; Medder, L.; Mailhot, B.; Morlat Therias, S.; Gardette, J. L. *Polymer* **2005**, *46*, 3571.
44. Morlat Therias, S.; Mailhot, B.; Gardette, J. L.; Da Silva, C.; Haidar, B.; Vidal, A. *Polym. Degrad. Stab.* **2005**, *90*, 78.
45. Morlat Therias, S.; Fanton, E.; Tomer, N. S.; Rana, S.; Singh, R. P.; Gardette, J. L. *Polym. Degrad. Stab.* **2006**, *91*, 3033.
46. Huaili, Q.; Zhenguang, Z.; Meng, F.; Fangling, G.; Shimin, Z.; Mingshu, Y. *J. Appl. Polym. Sci. Part B: Polym. Phys.* **2004**, *42*, 3006.
47. Dintcheva, N. T.; Al Malaika, S.; La, M. F. P. *Polym. Degrad. Stab.* **2009**, *94*, 1571.
48. Personal communication.
49. Yang, M.; Wang, K.; Ye, L.; Mai, Y. W.; Wu, J. *Plast. Rubber. Compos.* **2003**, *32*, 21.
50. Ashurov, N. R.; Sadykov, S. G.; Dolgov, V. V. *Polym. Sci. Ser. A* **2012**, *54*, 1403.
51. Zhao, C.; Feng, M.; Gong, F.; Qin, H.; Yang, M. *J. Appl. Polym. Sci.* **2004**, *93*, 676.